Supporting Information

Magnetic Nanoparticle as a Tool for Remote DNA Manipulations at a Single-Molecule Level

Aleksey A. Nikitin[1,2,*], Anton Yu. Yurenya[2,3], Timofei S. Zatsepin[2,4], Ilya O. Aparin[4], Vladimir P. Chekhonin[5], Alexander G. Majouga[1,2,6], Michael Farle[7], Ulf Wiedwald[7], Maxim A. Abakumov[1,5,#]

[1]National University of Science and Technology (MISIS), Moscow 119049, Russia
[2]M.V. Lomonosov Moscow State University, Moscow 119991, Russia
[3]National Research Center "Kurchatov Institute", Moscow 123098, Russia
[4]Skolkovo Institute of Science and Technology, Moscow 121205, Russia
[5]Department of Medical Nanobiotechnology, N.I. Pirogov Russian National Research Medical University, Moscow 117997, Russia
[6]D. Mendeleev University of Chemical Technology of Russia, Moscow 125047, Russia
[7]Faculty of Physics and Center for Nanointegration Duisburg-Essen, University of Duisburg-Essen, Duisburg, 47057, Germany

E-mail: [*]nikitin.aa@misis.ru; [#]abakumov_ma@rsmu.ru

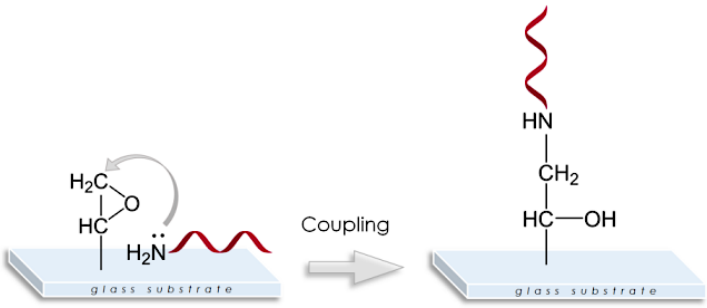

Fig. S1. Schematic representation of epoxy-activated microarray binding with SSO-targets.

I. Fabrication of MNP-oligo

The monodisperse hydrophobic MNPs@OA were synthesized by thermal decomposition of iron (III) oleate at 320 ºC in 1-octadecene in the presence of oleic acid and sodium oleate as surfactants. The determined hydrodynamic (HD) size of MNPs@OA in hexane was 21±2 nm. This value is two times higher than the MNP core size estimated by TEM analysis (11±2 nm). Such trend was also observed in previous works and can be explained by the contribution of oleic acid layers binding on the surface of nanoparticles to the overall HD size[1]. Since after synthesis MNPs@OA were hydrophobic, additional surface modification procedures were performed to stabilize them in aqueous media. At the first stage, the MNPs@OA surface was modified with 3,4-dixydroxyphenylacetic acid (MNPs@DOPAC) molecules by the ligand exchange protocol. The DOPAC molecules form strong covalent bonds between the oxygen atoms of hydroxyl groups and the Fe atoms of MNPs [2]. After replacing the oleic acid molecules on the MNP surface with DOPAC molecules the HD size decreased to 16±2 nm in deionized (DI) water, which is expected since the DOPAC molecule is much smaller than oleic acid[3]. Nevertheless, despite a small HD size and negative surface charge of MNPs@DOPAC (-30 mV), they were stable only in pure distilled water and almost instantly aggregated when the ionic strength of the solution was increased (**Fig. S2 and Table S2**). To improve solubility, MNPs@DOPAC were additionally conjugated with amino-carboxy polyethylene glycol (PEG) derivative (MNPs@DOPAC@PEG) using carbodiimide coupling chemistry. This step led to the stabilization of MNPs in various salt buffers like PBS, while their HD size increased from 16±2 to 24±3 nm. This phenomenon can be explained by the appearance of an additional charge and PEG chain steric repulsions[4]. Of note, the established PEG layer thickness was approximately 4 nm and is in line with previous works[5] (**Fig. S3 and Table S3).** At the last stage, MNPs@DOPAC@PEG were covalently conjugated with SSO-probe (MNP-oligo) also using carbodiimide coupling chemistry (**Table S4).** Moreover, by varying the concentration of SSO probe, we fixed 2 (MNP-oligo-2) and 12 (MNP-oligo-12) molecules of SSO-probe per single MNP. In addition, we investigated the aggregative stability of MNP-oligo-12 in various salt buffers by time-dependent HD measurements (**Fig. S4**). The obtained results showed that nanoparticles keep their stability even after 3 hours in NaCl, PBS and in DPBS and HBSS containing Ca^{2+} and Mg^{2+} ions.

Table S1. The main components of various salt buffers used in the work.

Components (mM)	Buffer			
	NaCl	**PBS**	**DPBS**	**HBSS**
Sodium Chloride	137	137	137	137
Potassium Chloride	-	2.7	2.7	5
Phosphate	-	10	10	7
Calcium Chloride	-	-	1	1
Magnesium Chloride	-	-	0.5	0.5
Magnesium Sulfate	-	-	-	0.4
Glucose	-	-	-	6
Sodium hydrocarbonate	-	-	-	4

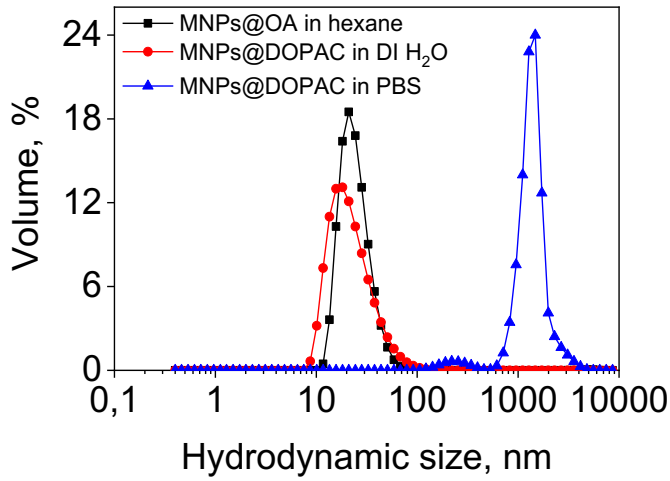

Fig. S2. Hydrodynamic curves of MNPs and their conjugates.

Table S2. The main hydrodynamic parameters and ζ-potential of MNPs and their conjugates.

Sample	Magnetic core size, nm	Hydrodynamic size, nm	Polydispersity index	ζ-potential, mV
MNPs@OA in hexane	11 ± 2	21 ± 2	0.215	-
MNPs@DOPAC in DI H_2O	11 ± 2	16 ± 2	0.221	-30
MNPs@DOPAC in PBS	11 ± 2	1484	0.576	-32

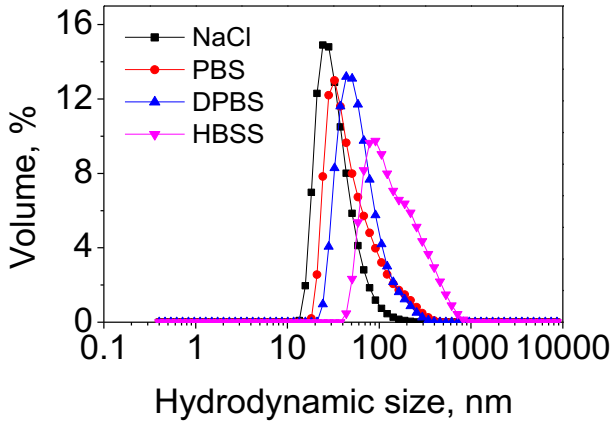

Fig. S3. Hydrodynamic curves of MNPs@DOPAC@PEG in various salt buffers.

Table S3. The main hydrodynamic parameters and ζ-potential of MNPs@DOPAC@PEG.

Buffer	Magnetic core size, nm	Hydrodynamic size, nm	Polydispersity index	ζ-potential, mV
NaCl	11 ± 2	24 ± 3	0.210	-12
PBS	11 ± 2	33 ± 2	0.206	-11
DPBS	11 ± 2	38 ± 4	0.230	-13
HBSS	11 ± 2	91 ± 3	0.235	-12

Table S4. The main hydrodynamic parameters and ζ-potential of MNP-oligo-12.

Buffer	Magnetic core size, nm	Hydrodynamic size, nm	Polydispersity index	ζ-potential, mV
NaCl	11 ± 2	26 ± 3	0.234	-14
PBS	11 ± 2	28 ± 2	0.216	-13
DPBS	11 ± 2	26 ± 3	0.203	-15
HBSS	11 ± 2	30 ± 3	0.227	-13

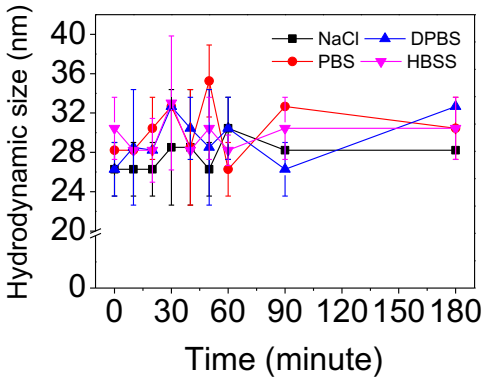

Fig. S4. MNP-oligo-12 stability assay based on hydrodynamic size measuring for 180 min by DLS in various salt buffers. The iron concentration was [Fe] = 0.2 mg/mL (n = 3 for each buffer) in all samples.

II. Quantifying the number of SSO-probe molecules fixed on a single MNP

The QuantiFluor® ssDNA Dye (Promega) was used to determine the number of SSO-probe molecules fixed on single MNPs. As a result, a calibration curve of the ssDNA Dye fluorescence intensity dependence on the SSO-probe concentration in solution was obtained (**Fig. S5**). We observed the well-known effect of partial quenching of fluorescence for SSO-probe that resulted in underestimating the analyte concentration[6]. The ssDNA Dye emission maximum is observed at 528 nm, but the absorbance values of the MNP solutions simultaneously increase linearly with increasing concentration at this wavelength (**Fig. S6**). It was found that the ssDNA Dye fluorescence intensity upon binding to the SSO-probe molecules in the MNPs@DOPAC@PEG solution (0.3 mg/mL) decreases 1.6 times compared with the fluorescence intensity of the same dye upon binding to SSO-probe in an MNP-free buffer. In contrast, when the concentration of MNPs@DOPAC@PEG was reduced to 0.2 mg/mL, the ssDNA Dye fluorescence quenching was not observed after binding to SSO-probe, which is explained by the insignificant absorbance of the nanoparticle solution at this concentration and a wavelength of 528 nm.

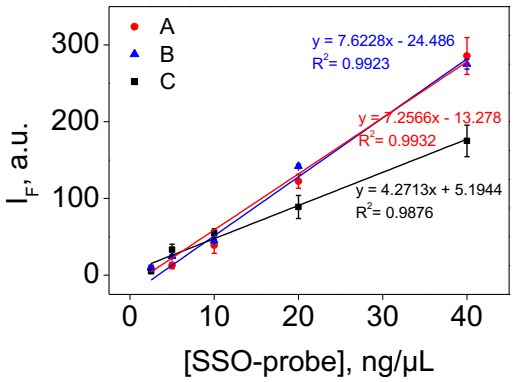

Fig. S5. Dependence of the QuantiFluor® ssDNA Dye fluorescence intensity on the SSO-probe concentration in DI H_2O (A), MNPs@DOPAC@PEG solution with $[Fe_3O_4]$ = 0.2 mg/mL (B) and MNPs@DOPAC@PEG solution with $[Fe_3O_4]$ = 0.3 mg/mL (C) (*n* = 3).

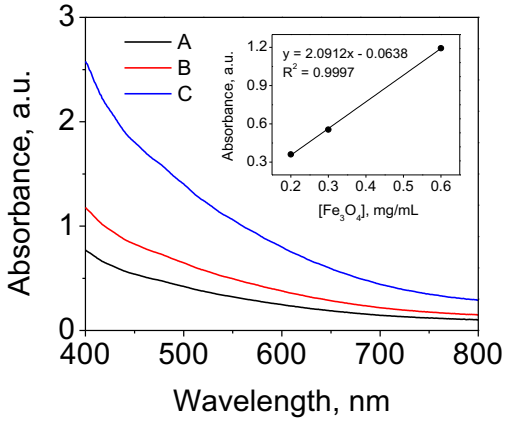

Fig. S6. Dependence of the MNPs@DOPAC@PEG solution absorbance on its concentration: 0.2 mg/mL (A), 0.3 mg/mL (B), 0.6 mg/mL (C) in terms of Fe_3O_4 in the wavelength range 400 – 800 nm, and a fitting curve (inset) for absorbance at 528 nm.

The total volume occupied by 1 mg of MNPs (excluding organic shell):

$$V_{MNPs} = \frac{m_{MNPs}}{\rho_{Fe_3O_4}} \quad (1)$$

$$m_{MNPs} = 1 \text{ mg} \Rightarrow V_{MNPs} = 192.3 \cdot 10^{15} \text{ nm}^3,$$

where $\rho_{Fe_3O_4}$= 5.2 g/cm^3 is the magnetite density[7].

The volume of a single MNP calculated according to TEM analysis:

$$V_{1\,MNP} = \left(\frac{b}{\sqrt{2}}\right)^3 = 470 \text{ nm}^3 \quad (2)$$

where b = 11 nm – the cube face diagonal of the MNPs determined from TEM images.

The number of MNPs in 1 mg of Fe_3O_4:

$$N_{MNPs} = \frac{V_{MNPs}}{V_{1\,MNP}} = 4.1 \cdot 10^{14} \quad (3)$$

The number of SSO-probe molecules per 1 mg of Fe_3O_4 MNPs:

$$N_{SSO-probe} = n_{SSO-probe} \cdot N_A \quad (4),$$

where $n_{SSO\text{-}probe}$ – amount of SSO-probe molecules per 1 mg of MNPs, $N_A = 6.02 \cdot 10^{23}$– Avogadro's number.

From **Fig. S5** for two types of MNP-oligo we obtained $n^{(1)}_{SSO-probe} = 1.20 \pm 0.06$ nmol and $n^{(2)}_{SSO-probe} = 8.33 \pm 0.34$ nmol of SSO-probe per 1 mg of MNPs, respectively ($M_{SSO-probe} = 20{,}535$ g/mol).

Hence, $N^{(1)}_{SSO-probe} = (7.2 \pm 0.4) \cdot 10^{14}$ and $N^{(2)}_{SSO-probe} = (50.1 \pm 2.1) \cdot 10^{14}$

The number of SSO-probe molecules per single MNP:

$$N_{SSO-probe}(per\ 1\ MNP) = \frac{N_{SSO-probe}}{N_{MNPs}} \quad (5)$$

$N^{(1)}_{SSO-probe}(per\ 1\ MNP) \sim 1.8 \pm 0.1$ (molecules) and $N^{(2)}_{SSO-probe}(per\ 1\ MNP) \sim 12.2 \pm 0.5$ (molecules)

Since any excess of free SSO-probe molecules in MNP-oligo solution can result in false-positive analysis, we ensure firm binding to the MNPs. To check this, we incubated 1 mL of each type of MNP-oligo (1 mg Fe_3O_4/mL) in a hybridization buffer (Arrayit®) for 3 h at 62°C and then

centrifuged the solutions through a 100 kDa pore-size filter to separate MNPs from the medium. Each resulting MNP precipitate was dispersed in 1 mL of PBS, and the fractions were then analyzed fluorometrically using QuantiFluor® ssDNA Dye. The obtained results showed that the respective concentrations of SSO-probe in MNP-oligo-2 (MNP-oligo-12) solutions were 1.21 ± 0.87 μM (8.29 ± 0.33 μM), and 0.05 ± 0.03 μM (0.09 ± 0.01 μM) in the filtered medium (**Fig. S7**). Thus, taking into account the initial concentrations of SSO-probe, we can conclude that the conjugates are stable and there is no leakage of SSO-probe from MNP-oligo was observed.

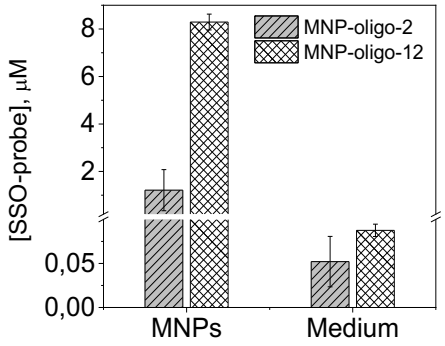

Fig. S7. Stability assay of MNP-oligo showing the concentration of SSO-probe in the MNP solutions and in the media after incubation of 1 mL of MNP-oligo-2 and MNP-oligo-12 ([Fe_3O_4] = 1 mg/mL) in hybridization buffer (Arrayit®) for 3 h at 62°C (n = 3).

III. Physical characterization of MNPs and their conjugates

Successful modification of the MNP surface with various ligands after each synthesis step was proven using Fourier transform infrared (FTIR) spectroscopy (**Fig. S8b**). An intense and wide band at 580 cm^{-1} in all spectra is the characteristic vibration of the Fe–O bond in iron oxide MNPs [8]. In the FTIR spectrum of MNPs@OA (**Fig. S8b (1)**) the main series of peaks is associated to oleic acid on the surface of MNPs: asymmetric (1560 cm^{-1}) and symmetric (1445 cm^{-1}) stretching modes of carboxyl (COO−) groups; the doublet consisting of two peaks at 2921 cm^{-1} and 2851 cm^{-1} and associated with asymmetric and symmetrical stretching modes of the CH_2 fragment; vinyl group vibrations =C–H at 3005 cm^{-1}, as well as a peak at 1423 cm^{-1}, which is most likely due to the formation of iron carboxylate during coordination of oleic acid molecules on the MNP surface [9,10]. Vibrations at 3427 cm^{-1} are due to the presence of water molecules in the probes. After the replacement of oleic acid molecules on the MNP surface with DOPAC molecules the asymmetric (1560 cm^{-1}) and symmetric (1445 cm^{-1}) vibrations of carboxyl groups disappeared (**Fig. S8b (2)**). On the contrary, a peak at 1630 cm^{-1} characterizing the carboxyl group vibrations in the DOPAC molecules appeared in the spectrum. The successful conjugation of MNPs with a PEG derivative is evidenced by the presence of C–O–C bond vibrations at 1100 cm^{-1}, as well as the amide bond and the C=O fragment in the spectrum at 1640 cm^{-1} and 1740 cm^{-1} respectively (**Fig. S8b (3)**)[11].

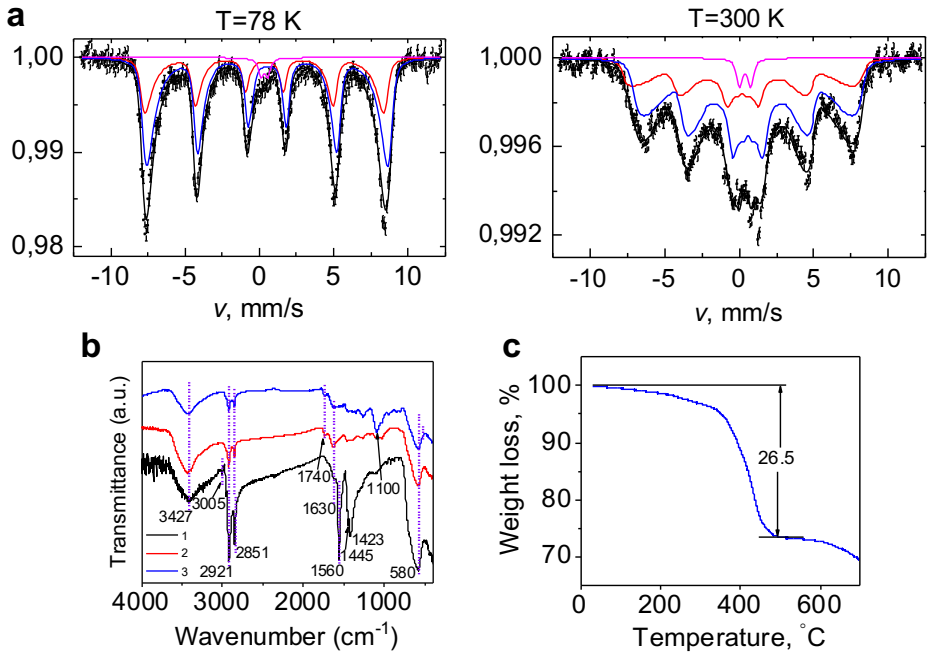

Fig. S8. Characterization of MNPs and their conjugates. a, Mössbauer absorption spectra of MNPs@OA, measured at liquid nitrogen temperature (78K, left) and room temperature (300K, right). The partial absorption spectra corresponding to the sublattice magnetizations M1 (red lines) and M2 (blue lines) are shown [12,13]. **b,** The FTIR spectra of MNPs: (1) MNPs@OA, (2) MNPs@DOPAC, (3) MNPs@DOPAC@PEG. **c,** Thermogravimetric curve of MNPs@OA.

Table S5. Calculated Mössbauer spectral parameters.

78K	**300K**
Model spectra	**Model spectra**
H_{hf1}=51.9(3) T	H_{hf1}=50.0(3) T
IS_1=0.35(4) mm/s	IS_1=0.24(3) mm/s
H_{hf2}=52.8(3) T	H_{hf2}=48.0(2) T
IS_2=0.54(2) mm/s	IS_2=0.58(2) mm/s
2q=QS*=0.3(2) mm/s	2q=QS*=0.41(5) mm/s

I – number of components, IS – isomer shift; QS – quadruple splitting; H_{hf} – hyperfine field

The specific magnetization values of MNPs were recalculated to the pure magnetic phase using thermogravimetric analysis in the temperature range 30 – 500°C (**Fig. S8c**). The first region with a mass loss of about 6.5% is observed up to 300°C and is explained by the loss of physically adsorbed water molecules, hexane and isopropanol, as well as oleic acid molecules weakly bonded to the surface of MNPs. The second region with a mass loss of about 20% falls on the temperature range 300 – 500 ºC and is explained by the loss of oleic acid molecules covalently bonded to the surface of MNPs [14]. A decrease in the sample mass at temperatures above 500°C is most likely associated with the processes of MNPs phase transformation [3].

IV. Immobilization of SSO-targets on the glass surface and hybridization to complementary SSO-probes.

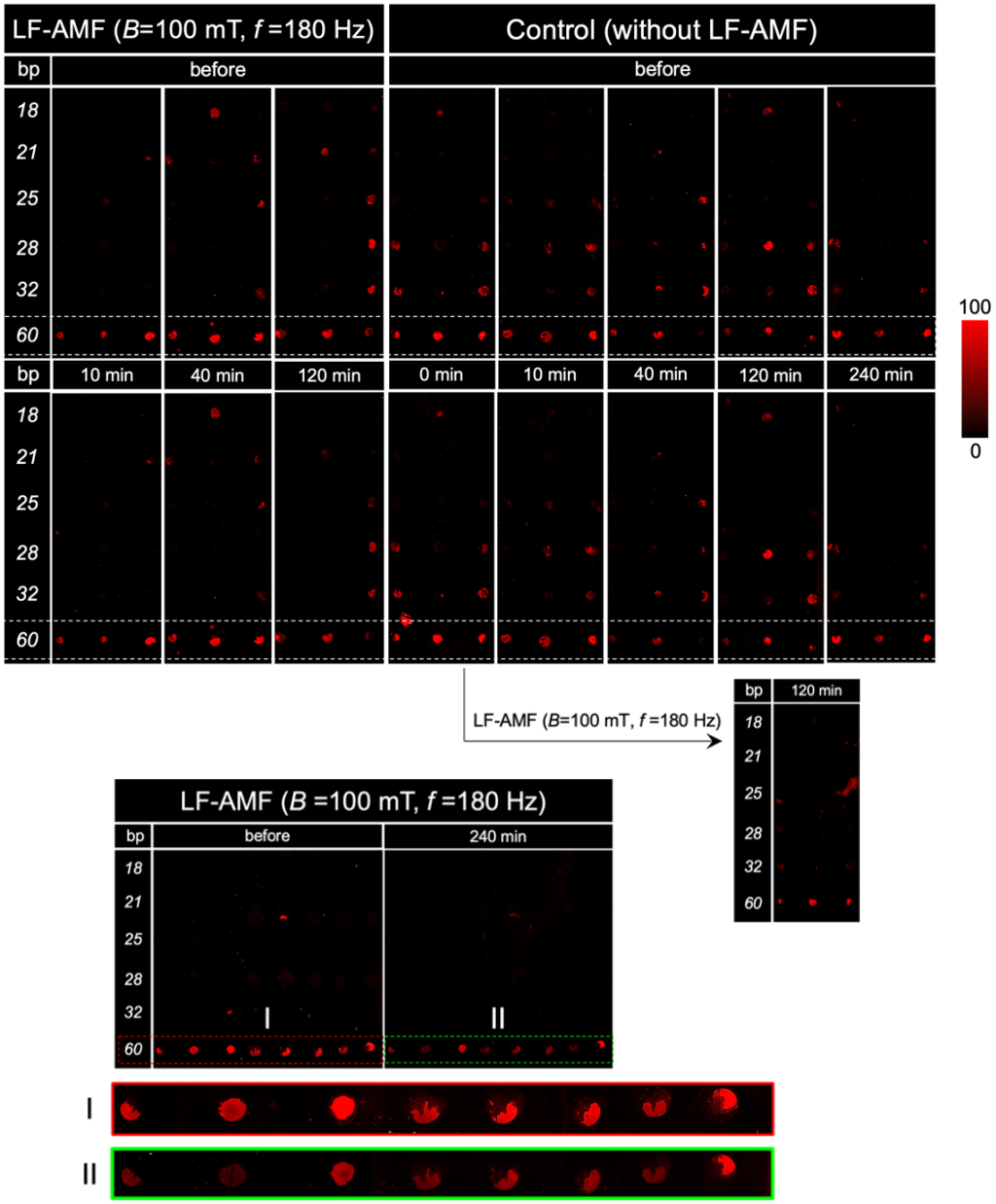

Fig. S9. Representative images of the microarrays formed using MNP-oligo-2 before and after treatment by the LF-AMF (f = 180 Hz, B = 100 mT).

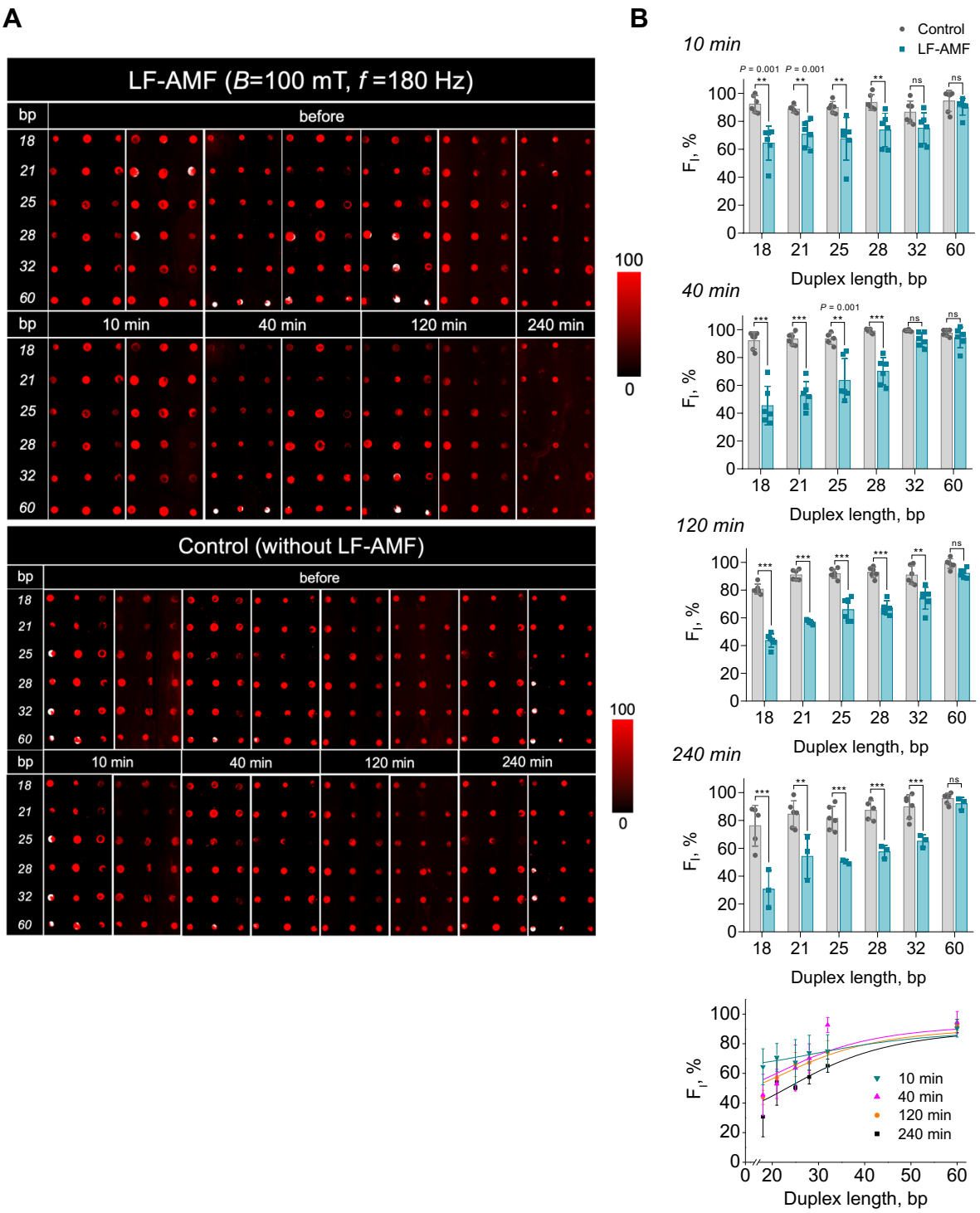

Fig. S10. The influence of the LF-AMF (f = 180 Hz, B = 100 mT) on the cleavage of DNA duplexes in time for MNP-oligo-12. **A,** Representative images of the microarrays before and after treatment with the LF-AMF. **B,** Histograms of the sCy5 fluorescence intensity dependence on the length of duplexes treated by the LF-AMF for 10, 40, 120 and 240 min, respectively. Data are means ± SD. Statistical significance was calculated by one-way ANOVA test (**$P < 0.01$, ***$P < 0.001$, ns – non-significant).

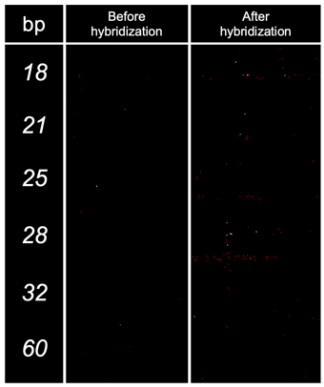

Fig. S11. Representative images of the microarray before and after hybridization procedure using MNPs@sCy5 solution containing 0.25 μM sCy5.

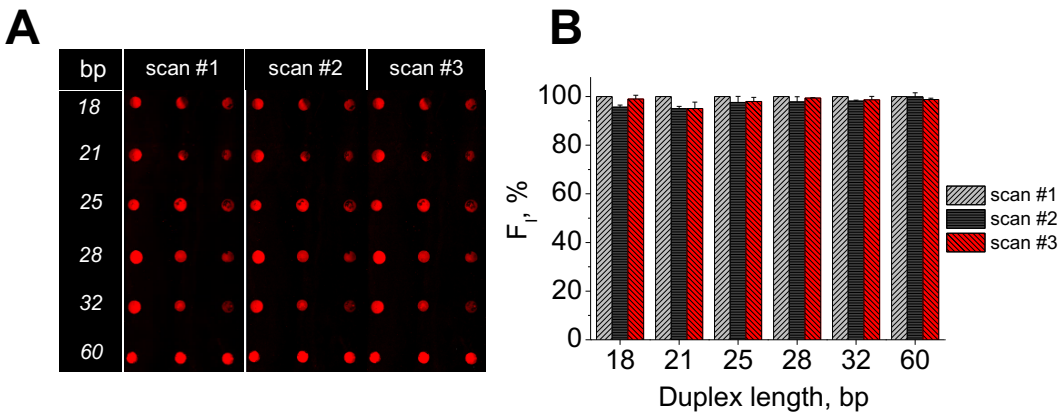

Fig. S12. A, Representative images of the microarray after three consecutive scans. **B**, Histogram of the sCy5 fluorescence intensity after each scan. Statistical significance was calculated by one-way ANOVA test (n = 3). There is no statistical significance in all cases.

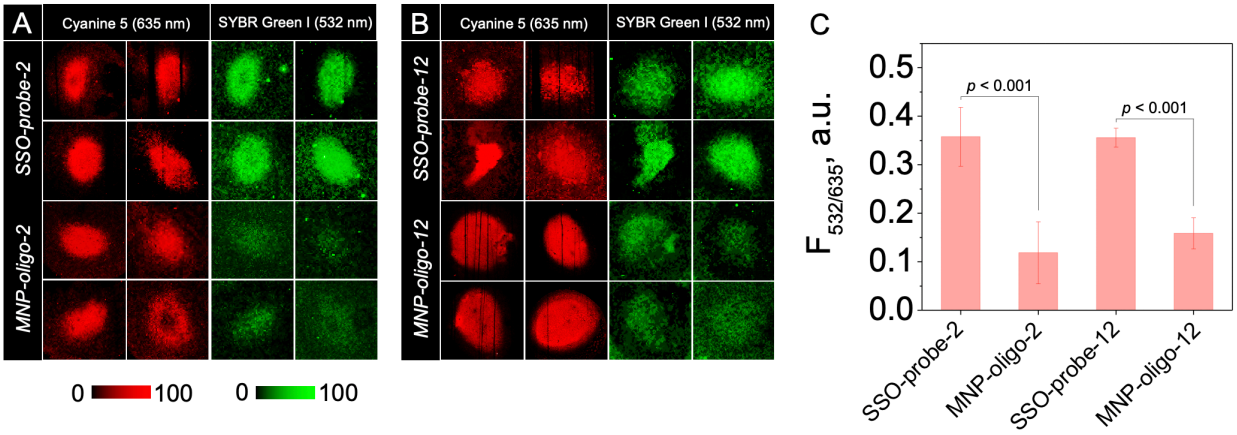

Fig. S13. (A, B) Representative fluorescent images of 60 nt microarrays after hybridization with pure SSO-probe or MNP-oligo and after staining with SYBR Green I. The concentration of pure SSO-probe and MNP-oligo during hybridization was normalized to the SSO probe content. (C) Histogram of the normalized 532 nm/635 nm fluorescence intensity. Statistical significance was calculated by one-way ANOVA test (n = 4).

V. Theoretical substantiation of the magneto-mechanical effect mediated by individual MNP in LF-AMF.

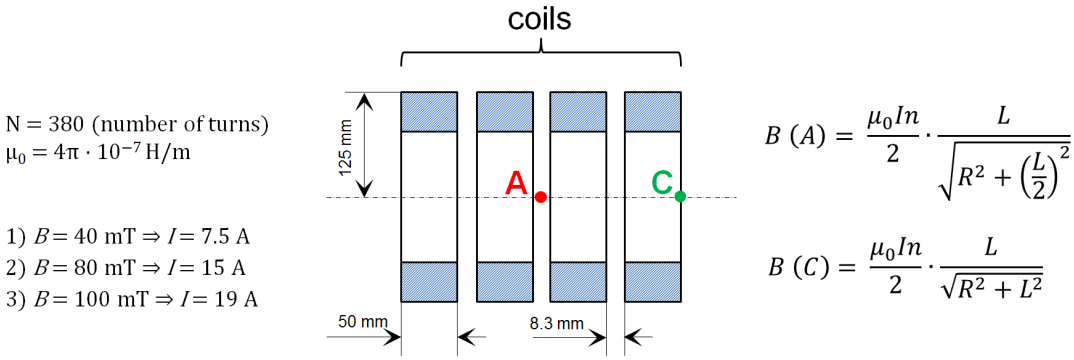

Fig. S14. Schematic representation of the LF-AMF magnetic coils with indicating of their main parameters. The gradient of the magnetic field between the points of the coil (A and C) does not exceed 4%. Taking into account that the microarray is 2 cm wide and is placed in the central region (point A), the value of the gradient is negligible and does not exceed 0.1% ($\nabla B \sim 0.1$ mT·m^{-1} at B = 100 mT).

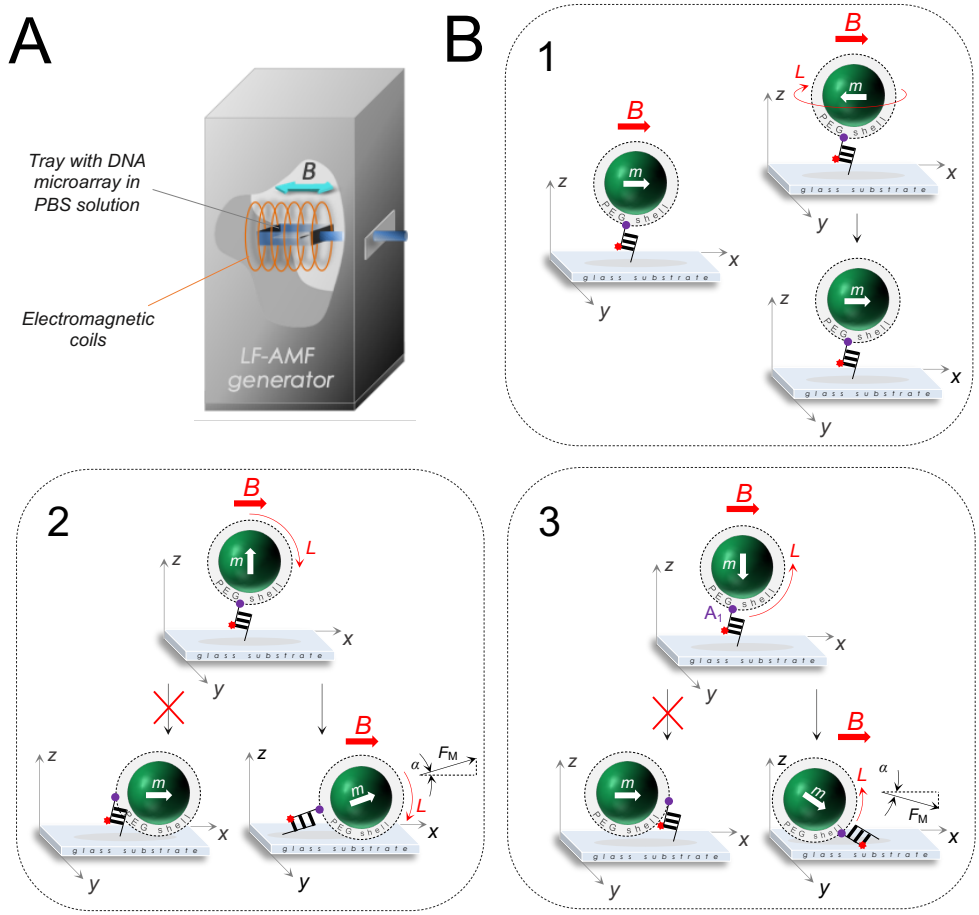

Fig. S15. Schematic illustration of the magneto-mechanical effects mediated by individual MNP in the LF-AMF. (A) The scheme of the LF-AMF generator. **(B)** Possible routes of Brownian MNP oscillation in the LF-AMF.

In our case the torque L exerted on each MNP mediates the stretching force F_M that occurs when the angular frequency $\omega = 2\pi f$ of the LF-AMF is significantly less than the critical frequency (ω_c) of the MNP [15]. In this case MNPs undergo rotational movements after each change of the induction vector orientation of external LF-AMF. The critical frequency ω_c can be expressed as:

$$\omega_C = \frac{mB}{6\eta V_{HD-MNP}}$$

where $m = M(B)\cdot\rho\cdot V$ is the magnetic moment of a single domain MNP, B –amplitude of the LF-AMF, ρ – density, V – magnetic volume, η – medium viscosity, $V_{HD\text{-}MNP}$ – hydrodynamic volume of an MNP; $M(B)$ – specific magnetization of an MNP in the external magnetic field B.

In the equation all parameters are constant except the amplitude of the external LF-AMF. Thus, the critical frequency is the linear function of the magnetic field amplitude. Experimentally, we determined a magnetization of $0.73\cdot M_S = 48.2$ A·m^2·kg^{-1} in $B = 100$ mT. This leads to an average magnetic moment per MNP of $m = 48.2$ A·m^2·kg^{-1} · 5200 kg·m^{-3} · $(7.8\cdot10^{-9}$ m$)^3 = 1.18\cdot10^{-19}$ A·m^2 with $V = a^3 = (11/2^{0.5})^3$ – volume of the MNP. The factor $2^{0.5}$ accounts for the edge length of the cubic MNPs. The parameters in the denominator are the dynamic viscosity of PBS solution $\eta = 0.89\cdot10^{-3}$ Pa·s at 25 °C and the hydrodynamic volume $V_{HD\text{-}MNP} = (\pi/6)\cdot d_{HD\text{-}MNP}^3 = 1.15\cdot10^{-23}$ m^3 using the experimental hydrodynamic diameter of 28 nm. With these values we determined the critical angular frequency $\omega_c = 1.92\cdot10^5$ rad·s^{-1}, which corresponds to about $f_C = 30$ kHz. In the LF-AMF experiments used for DNA duplex cleavage the frequency was set to $f = 180$ Hz. Thus, $f << f_C$ and in turn, the oscillation amplitude $\Delta\varphi = \pi$, which means that the magnetization of the MNPs follows the external field[15].

The value of the hydrodynamic force F_{HD} acting upon the oligonucleotide duplex is negligible here due to the small viscosity of the PBS medium ($\eta = 0.89\cdot10^{-3}$ Pa · s). This force linearly depends on the solvent viscosity and the flow velocity according to Stokes' equation [16]:

$$F_{HD} = 6\pi\eta R_{mol} v$$

where, η – medium viscosity, R_{mol} – hydrodynamic radius of the oligonucleotide duplex anchored to the MNP, v – the flow velocity relative to the object.

The flow velocity v can be expressed as a product of the LF-AMF instant angular frequency $\omega = 2\pi f$ and the MNP hydrodynamic radius $R_{HD\text{-}MNP}$ [15] where $f = 180$ Hz is the frequency used in the experiments. This force is proportional to the molecule radius anchored to the MNP. For simplicity, we consider the 60 bp duplex as a spherical globule with a radius of ~13 nm [17]. This leads to the hydrodynamic force $F_{HD} = 12\pi^2\eta f R_{mol} R_{HD\text{-}MNP} = 12\cdot\pi^2\cdot0.89\cdot10^{-3}$ Pa·s · 180 s^{-1} · $13\cdot10^{-9}$ m · $14\cdot10^{-9}$ m = 0.003 pN.

Of note, up to date, there is still no clear understanding of the magnitude of the magneto-mechanical stretching F_M force, which single iron oxide MNP mediate in an external static gradient field or an oscillating magnetic field. Direct comparison of results from different studies is complicated as any modification in the shape, size, phase composition, type of surface-active stabilizers of MNPs may strongly alter their physical and chemical properties, e.g., stability in water and buffers, surface area, or magnetic susceptibility. For example the identical maximum magnetically driven stretching force $F_M = 3\cdot10^{-11}$ N was calculated for iron oxide 500 nm MNPs

[18] and for 50 nm Zn-doped iron oxide MNPs [19]. The tension force for 45 nm cubic silica-coated iron oxide MNP was estimated to be $1 \cdot 10^{-13}$ N in oscillating magnetic field with magnetic field gradient of 10^3 T/m [20], whereas the same F_M value was obtained for 5 nm iron oxide MNPs at field gradient of 10^4 T/m [21]. Also, it was previously shown that the aggregates of 20 nm iron oxide MNPs mediate a tension force of $(6 \pm 2) \cdot 10^{-8}$ N by applying a small magnetic field gradient of 120 T/m [22], while similar aggregates of 50 nm iron oxide MNPs produce the tension force up to $1 \cdot 10^{-7}$ N under the filed gradients of 2,500 T/m to 70,000 T/m [23]. In another work, the tension force of $1 \cdot 10^{-17}$ N was calculated for 5 nm superparamagnetic iron oxide MNPs at applied external field B = 0.1 T [24]. Thus, a comparison of these results does not allow one to establish an unambiguous correlation "MNP core size – maximum value of mediated F_M".

VI. Experimental study of the DNA duplex cleavage

In the quasi-static mode, the value of a local overheating on MNP surface relative to the surrounding medium can be expressed as [25]:

$$\Delta T_S = \frac{q D_{MNP}^2 \rho}{12\lambda}$$

where q is a SAR value of MNPs, D_{MNP} – diameter of the magnetic core, ρ – density of the magnetic core and $\lambda \approx 0.6$ W·(m·K)$^{-1}$ – thermal conductivity coefficient of water.

Taking into account that the typical value of q is 100 – 1000 W·g^{-1} in a regular field with B = 25 – 40 mT and f = 200 – 500 kHz, and also $q \sim fH^2$, we obtain in our conditions (B = 100 mT, f = 180 Hz) q = 0.2 – 2 W·g^{-1}. Consequently, the maximum local overheating is calculated as:

$$\Delta T_S = \frac{2\ \mathrm{W \cdot g^{-1}} \cdot 11^2 \cdot (10^{-9})^2 \cdot \mathrm{m^2} \cdot 5200\ \mathrm{kg \cdot m^{-3}}}{12 \cdot 0.6\ \mathrm{W \cdot (m \cdot K)^{-1}}} = 1.7 \cdot 10^{-10}\mathrm{K}$$

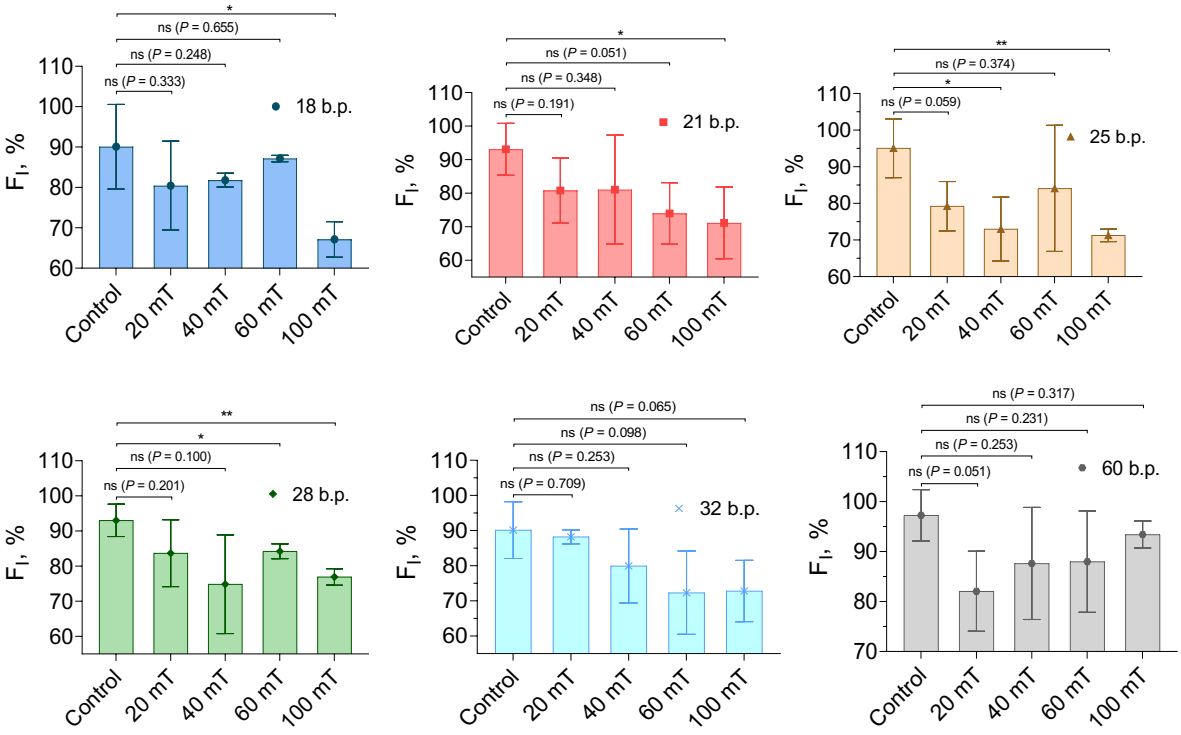

Fig. S16. The histograms of the sCy5 fluorescence intensity after treatment of duplexes (18 – 60 bp) formed using MNP-oligo-12 by the LF-AMF (f = 180 Hz, τ = 10 min) at various field amplitudes. Data are means ± SD. Statistical significance was calculated by one-way ANOVA test (n = 3, *P < 0.05, **P < 0.01, ns – non-significant).

VII. Supplementary References

(1) Lim, J.; Yeap, S. P.; Che, H. X.; Low, S. C. Characterization of Magnetic Nanoparticle by Dynamic Light Scattering. *Nanoscale Res. Lett.* **2013**, *8* (1), 1–14.

(2) Amstad, E.; Gillich, T.; Bilecka, I.; Textor, M.; Reimhult, E. Ultrastable Iron Oxide Nanoparticle Colloidal Suspensions Using Dispersants with Catechol-Derived Anchor Groups. *Nano Lett.* **2009**, *9* (12), 4042–4048.

(3) Yang, K.; Peng, H.; Wen, Y.; Li, N. Re-Examination of Characteristic FTIR Spectrum of Secondary Layer in Bilayer Oleic Acid-Coated Fe 3 O 4 Nanoparticles. *Appl. Surf. Sci.* **2010**, *256* (10), 3093–3097.

(4) Tirosh, O.; Barenholz, Y.; Katzhendler, J.; Priev, A. Hydration of Polyethylene Glycol-Grafted Liposomes. *Biophys. J.* **1998**, *74* (3), 1371–1379.

(5) Spadaro, D.; Iatì, M. A.; Donato, M. G.; Gucciardi, P. G.; Saija, R.; Cherlakola, A. R.; Scaramuzza, S.; Amendola, V.; Maragò, O. M. Scaling of Optical Forces on Au-PEG Core-Shell Nanoparticles. *RSC Adv.* **2015**, *5* (113), 93139–93146.

(6) Zeug, A.; Woehler, A.; Neher, E.; Ponimaskin, E. G. Quantitative Intensity-Based FRET Approaches - A Comparative Snapshot. *Biophys. J.* **2012**, *103* (9), 1821–1827.

(7) Lide, D. R. *CRC Handbook of Chemistry and Physics 86TH Edition 2005-2006*; 2005.

(8) Waldron, R. D. Infrared Spectra of Ferrites. *Phys. Rev.* **1955**, *99* (6), 1727–1735.

(9) Roonasi, P.; Holmgren, A. A Fourier Transform Infrared (FTIR) and Thermogravimetric Analysis (TGA) Study of Oleate Adsorbed on Magnetite Nano-Particle Surface. *Appl. Surf. Sci.* **2009**, *255* (11), 5891–5895.

(10) Perez De Berti, I. O.; Cagnoli, M. V.; Pecchi, G.; Alessandrini, J. L.; Stewart, S. J.; Bengoa, J. F.; Marchetti, S. G. Alternative Low-Cost Approach to the Synthesis of Magnetic Iron Oxide Nanoparticles by Thermal Decomposition of Organic Precursors. *Nanotechnology* **2013**, *24* (17).

(11) Park, J. Y.; Daksha, P.; Lee, G. H.; Woo, S.; Chang, Y. Highly Water-Dispersible PEG Surface Modified Ultra Small Superparamagnetic Iron Oxide Nanoparticles Useful for Target-Specific Biomedical Applications. *Nanotechnology* **2008**, *19* (36).

(12) Chuev, M. A. Novel Models of Magnetic Dynamics for Characterization of Nanoparticles Biodegradation in a Body from Mössbauer and Magnetization Measurements. *J. Magn. Magn. Mater.* **2019**, *470*, 12–17.

(13) Chuev, M. A. Excitation Spectrum of the Néel Ensemble of Antiferromagnetic Nanoparticles as Revealed in Mössbauer Spectroscopy. *Adv. Condens. Matter Phys.* **2017**, *2017*.

(14) Ozel, F.; Kockar, H.; Beyaz, S.; Karaagac, O.; Tanrisever, T. Superparamagnetic Iron Oxide Nanoparticles: Effect of Iron Oleate Precursors Obtained with a Simple Way. *J. Mater. Sci. Mater. Electron.* **2013**, *24* (8), 3073–3080.

(15) Golovin, Y. I.; Gribanovsky, S. L.; Golovin, D. Y.; Klyachko, N. L.; Majouga, A. G.; Master, A. M.; Sokolsky, M.; Kabanov, A. V. Towards Nanomedicines of the Future: Remote Magneto-Mechanical Actuation of Nanomedicines by Alternating Magnetic Fields. *J. Control. Release* **2015**, *219*, 43–60.

(16) McCann, M. P. Physical Chemistry CD (Laidler, Keith James; Meiser, John H.; Sanctuary, Bryan C.). *J. Chem. Educ.* **2003**, *80* (5), 489.

(17) Liphardt, J.; Onoa, B.; Smith, S. B.; Tinoco I., J.; Bustamante, C. Reversible Unfolding of Single RNA Molecules by Mechanical Force. *Science (80-.).* **2001**, *292* (5517), 733–737.

(18) Etoc, F.; Lisse, D.; Bellaiche, Y.; Piehler, J.; Coppey, M.; Dahan, M. Subcellular Control of Rac-GTPase Signalling by Magnetogenetic Manipulation inside Living Cells. *Nat. Nanotechnol.* **2013**, *8* (3), 193–198.

(19) Seo, D.; Southard, K. M.; Kim, J. W.; Lee, H. J.; Farlow, J.; Lee, J. U.; Litt, D. B.; Haas, T.; Alivisatos, A. P.; Cheon, J.; Gartner, Z. J.; Jun, Y. W. A Mechanogenetic Toolkit for Interrogating Cell Signaling in Space and Time. *Cell* **2016**, *165* (6), 1507–1518.

(20) Lee, J. H.; Kim, J. W.; Levy, M.; Kao, A.; Noh, S. H.; Bozovic, D.; Cheon, J. Magnetic Nanoparticles for Ultrafast Mechanical Control of Inner Ear Hair Cells. *ACS Nano* **2014**, *8* (7), 6590–6598.
(21) Zablotskii, V.; Lunov, O.; Dejneka, A.; Jastrabk, L.; Polyakova, T.; Syrovets, T.; Simmet, T. Nanomechanics of Magnetically Driven Cellular Endocytosis. *Appl. Phys. Lett.* **2011**, *99* (18), 183701.
(22) Desprat, N.; Supatto, W.; Pouille, P. A.; Beaurepaire, E.; Farge, E. Tissue Deformation Modulates Twist Expression to Determine Anterior Midgut Differentiation in Drosophila Embryos. *Dev. Cell* **2008**, *15* (3), 470–477.
(23) Tseng, P.; Judy, J. W.; Di Carlo, D. Magnetic Nanoparticle-Mediated Massively Parallel Mechanical Modulation of Single-Cell Behavior. *Nat. Methods* **2012**, *9* (11), 1113–1119.
(24) Mannix, R. J.; Kumar, S.; Cassiola, F.; Montoya-Zavala, M.; Feinstein, E.; Prentiss, M.; Ingber, D. E. Nanomagnetic Actuation of Receptor-Mediated Signal Transduction. *Nat. Nanotechnol.* **2008**, *3* (1), 36–40.
(25) Vlasova, K. Y.; Vishwasrao, H.; Abakumov, M. A.; Golovin, D. Y.; Gribanovsky, S. L.; Zhigachev, A. O.; Poloznikov, A.; Majouga, A. G.; Golovin, Y. I.; Sokolsky-Papkov, M.; Klyachko, N. L.; Kabanov, A. V. Enzyme Release from Polyion Complex by Extremely Low Frequency Magnetic Field. *Sci. Rep.* **2020**, *10*, 4745.